Analysis of Class DE Current Driven Low di/dt Rectifier

Yutaro Minami, *Student Member, IEEE*, and Hirotaka Koizumi, *Member, IEEE*

***Abstract*—Class DE current driven low di/dt rectifier satisfies Class E switching condition and low diode current stress, which is no more than the output current. Thus, the switching loss is decreased extremely. In this paper, the Class DE current driven low di/dt rectifier is analyzed for any diode-on-duty-ratio. The initial phase angle of the input current, the current and voltage transfer functions, the normalized input resistance and inductance, the normalized diode voltage stress, and the power-output capability are obtained, and clarified as the functions of the diode-on-duty ratio and those of R/wL. Moreover, the power conversion efficiency and the circuit design method are shown. The circuit performance has been confirmed by the simulation results and the experimental results. In the simulation and the experiment, the characteristics of the output voltage and the power conversion efficiency against the amplitude of the input current, the load resistance, and the operation frequency have been obtained. In addition, the relationship between the equations, simulation results, and experimental results have been obtained. Theoretical, simulation, and experimental results were in good agreement with each other.**

***Index Terms*—Class DE current driven low *di/dt* rectifier, zero current derivative switching (ZCDS), zero current switching (ZCS).**

I. Introduction

SWITCHED-MODE power supply is required downsizing, low cost, high efficiency, and low noise. To satisfy downsizing and low cost, the power converters are required to be operated in high frequency. However, the high-frequency operation increases the switching losses at switching devices, such as diodes or MOSFETs, which decrease the power conversion efficiency. In addition, the high-frequency operation causes the noise. To solve the efficiency and the noise problems in the diodes, Class D rectifiers [1]–[6], Class E rectifiers [5]–[33], and Class DE rectifiers [34]–[41] have been proposed. The features of Class D rectifiers, Class E rectifiers, and Class DE rectifiers are summarized in Table I.

Class D voltage driven half-wave rectifier [4]–[6], which is one of the Class D rectifiers, has the following features: the diodes turning on and off at zero-voltage switching (ZVS) and low dv/dt, and the low diode current stress, which is no more than the output current. However, the diodes turn on and off at high di/dt, which causes more switching losses in high frequency range.

Manuscript received September 23, 2014; revised November 21, 2014; accepted December 20, 2014. Date of publication January 6, 2015; date of current version August 21, 2015. Recommended for publication by Associate Editor M. A. E. Andersen.

The authors are with the Tokyo University of Science, Tokyo 125-8585, Japan (e-mail: Y.JP.M@ieee.org; littlespring@ieee.org).

Color versions of one or more of the figures in this paper are available online at http://ieeexplore.ieee.org.

Digital Object Identifier 10.1109/TPEL.2014.2387878

Class E current driven low di/dt rectifier [26]–[29], which is one of the Class E rectifiers, has the following features: the diodes turning on at zero-current switching (ZCS), zero-current derivative switching (ZCDS), ZVS, and low dv/dt, and turning off at ZCS and low di/dt. However, the diode current stress of the rectifier is high, which is several times higher than the output current.

Combining the properties of the Class D voltage driven half-wave rectifier and the Class E current driven low di/dt rectifier, Class DE current driven low di/dt rectifier [40] was proposed. The Class DE current driven low di/dt rectifier, which is one of the Class DE rectifiers, has the following features: the diodes turning on at ZCS, ZCDS, ZVS, and low dv/dt, and turning off at ZCS and low di/dt. Moreover, the diode current stress of the rectifier is low, which is no more than the output current. In [40], the equations of the voltage and current waveforms for the diodes and the inductor are derived.

In this paper, the Class DE current driven low di/dt rectifier is analyzed for any diode-on-duty-ratio. The initial phase angle of the input current, the current and voltage transfer functions, the normalized input resistance and inductance, the normalized diode voltage stress, and the power-output capability are obtained, and clarified as functions of the diode-on-duty ratio and those of R/wL. Moreover, the power conversion efficiency and the circuit design method are shown. The performance has been confirmed with the simulations and the circuit experiments. In the simulation and the experiment, the characteristics of the output voltage and power conversion efficiency against the amplitude of the input current, the load resistance, and the operation frequency have been obtained. In addition, the relationship between the derivations, simulation results, and experimental results have been obtained.

II. Circuit Description

Fig. 1(a) shows a circuit topology of the Class DE current driven low di/dt rectifier, which consists of two diodes D_1 and D_2, an inductor L, a filter inductor L_F, a filter capacitor C_F, and a load resister R. The filter inductor L_F and the filter capacitor C_F form a second-order low-pass output filter. The input current of the Class DE current driven low di/dt rectifier is an ac current source $i_{\rm IN}$, which supplies a sinusoidal current with an operating frequency f. Assuming that the filter inductance L_F is large enough to feed a constant current, the L_F–C_F output filter and the load resister R can be replaced by a dc current sink I_O. Fig. 1(b) shows an equivalent circuit of the Class DE current driven low di/dt rectifier.

Fig. 2 shows the idealized current and voltage waveforms in the Class DE current driven low di/dt rectifier, where $i_{\rm IN}$ is

TABLE I
CONVENTIONAL OF SOFT-SWITCHING RECTIFIER

Rectifier	Switching		Diode Current Stress	Diode Voltage Stress
	Turn On	Turn Off		
Class D current driven half wave rectifier [1]-[3], [5], [6]	ZCS, low di/dt high dv/dt		High	Low
Class D voltage driven half wave rectifier [4]-[6]	high di/dt ZVS, low dv/dt		Low	High
Class E current driven low dv/dt rectifier [7]-[18]	high di/dt ZVS, low dv/dt	ZCS, low di/dt ZVS, ZVDS	High	High
Class E voltage driven low dv/dt rectifier [19]-[25]				
Class E current driven low di/dt rectifier [26]-[29]	ZCS, ZCDS ZVS, low dv/dt	ZCS, low di/dt high dv/dt	High	High
Class E voltage driven low di/dt rectifier [30]-[33]				
Class DE current driven low dv/dt rectifier [34]-[39]	high di/dt ZVS, low dv/dt	ZCS, low di/dt ZVS, ZVDS	High	Low
Class DE current driven low di/dt rectifier [40]	ZCS, ZCDS ZVS, low dv/dt	ZCS, low di/dt high dv/dt	Low	High
Class DE voltage driven low di/dt rectifier [41]				

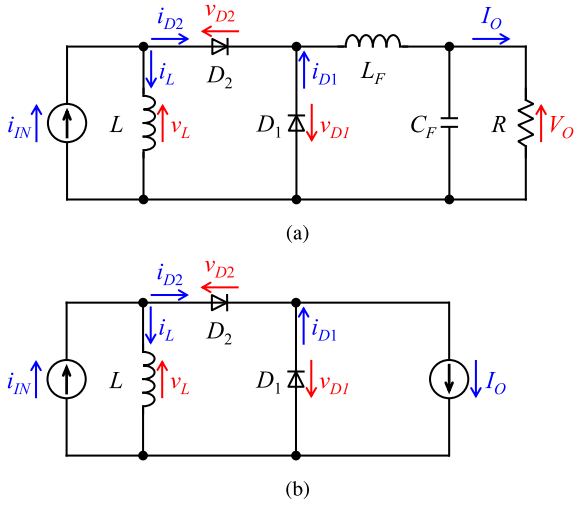

Fig. 1. Class DE current driven low di/dt rectifier. (a) Circuit diagram. (b) Equivalent circuit.

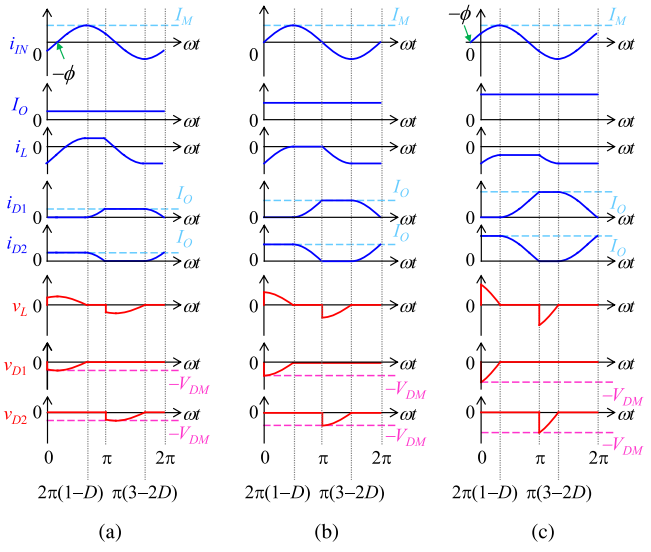

Fig. 2. Idealized current and voltage waveforms in the rectifier of Fig. 1. (a) $D < 0.75$. (b) $D = 0.75$. (c) $D > 0.75$.

the input current, I_M is the amplitude of the input current $i_{\rm IN}$, I_O is the output current, i_L is the current through the inductor L, v_L is the voltage across the inductor L, i_{D1} and i_{D2} are the currents through the diodes D_1 and D_2, v_{D1} and v_{D2} are the reverse voltages of the diodes D_1 and D_2, ϕ is the initial phase angle of the input current $i_{\rm IN}$, and D is the diode-on-duty ratio of the diodes D_1 and D_2.

From Fig. 2, the diodes D_1 and D_2 turn on at ZCS, ZCDS, ZVS, and low dv/dt, and turn off at ZCS and low di/dt; thus, resulting in low switching losses. Moreover, the diode current stress of the rectifier is no more than the output current I_O.

III. PRINCIPLE OF OPERATION

The principle of operation of the proposed circuit is explained under the following assumptions:

1) the rectifier is driven by an ideal sine-wave current source $i_{\rm IN}$;
2) the diodes D_1 and D_2 are the ideal devices, i.e., the diodes have zero threshold voltage, zero on-resistance, infinite off-resistance, and zero junction capacitance;
3) the filter inductance L_F is large enough to feed a constant current I_O;
4) all the circuit elements are ideal.

The operation of the rectifier is discussed in four states by the state of the diodes D_1 and D_2.

*State*1 $[0 \le \omega t \le 2\pi(1-D)]$

The diode D_1 is OFF and the diode D_2 is ON. Therefore, the current through the inductor L is

$$i_L = i_{\rm IN} - I_O. \tag{1}$$

Thus, the voltage across the inductor L is in sinusoidal shape. The reverse voltage of the diode D_1 is

$$v_{D1} = -v_L. \tag{2}$$

The current through the diode D_2 is

$$i_{D2} = I_O. \tag{3}$$

At $\omega t = 2\pi(1-D)$, the reverse voltage of the diode D_1 reaches zero and the diode D_1 turns on.

*State*2 $[2\pi(1-D) \le \omega t \le \pi]$

The diodes D_1 and D_2 are ON. Total of the currents through the diode D_1 and D_2 is the output current I_O

$$i_{D1} + i_{D2} = I_O \tag{4}$$

At $\omega t = \pi$, the current through the diode D_2 reaches zero and the diode D_2 turns off.

$State3\,[\pi \le \omega t \le \pi(3-2D)]$

The diode D_1 is ON and the diode D_2 is OFF. Therefore, the current through the inductor L is

$$i_L = i_{\mathrm{IN}}. \tag{5}$$

Thus, the voltage across the inductor L is in sinusoidal shape. The reverse voltage of the diode D_2 is

$$v_{D2} = v_L. \tag{6}$$

The current through the diode D_1 is

$$i_{D1} = I_O. \tag{7}$$

At $\omega t = \pi(3-2D)$, the reverse voltage of the diode D_2 reaches zero and the diode D_2 turns on.

$State4\,[\pi(3-2D) \le \omega t \le 2\pi]$

The diodes D_1 and D_2 are ON. Total of the currents through the diode D_1 and D_2 is the output current I_O

$$i_{D1} + i_{D2} = I_O. \tag{8}$$

At time $\omega t = 2\pi$, the current through the diode D_1 reaches zero and the diode D_1 turns off.

IV. Equation of Diodes and Inductor Waveforms

In [40], the equations of the diodes and the inductor waveforms have been derived for any diode-on-duty ratio. Here, we show the obtained waveform equations in [40]

$$i_{D1} = \begin{cases} 0, & [0 \le \omega t \le 2\pi(1-D)] \\ -\frac{I_O}{1+\cos 2\pi D}\left\{\sin\left[\omega t + \pi\left(2D-\frac{3}{2}\right)\right]-1\right\}, & [2\pi(1-D) \le \omega t \le \pi] \\ I_O, & [\pi \le \omega t \le \pi(3-2D)] \\ I_O - \frac{I_O}{1+\cos 2\pi D}\left\{\sin\left[\omega t + \pi\left(2D-\frac{3}{2}\right)\right]+1\right\}, & [\pi(3-2D) \le \omega t \le 2\pi] \end{cases} \tag{9}$$

$$i_{D2} = \begin{cases} I_O, & [0 \le \omega t \le 2\pi(1-D)] \\ I_O + \frac{I_O}{1+\cos 2\pi D}\left\{\sin\left[\omega t + \pi\left(2D-\frac{3}{2}\right)\right]-1\right\}, & [2\pi(1-D) \le \omega t \le \pi] \\ 0, & [\pi \le \omega t \le \pi(3-2D)] \\ \frac{I_O}{1+\cos 2\pi D}\left\{\sin\left[\omega t + \pi\left(2D-\frac{3}{2}\right)\right]+1\right\}, & [\pi(3-2D) \le \omega t \le 2\pi] \end{cases} \tag{10}$$

$$i_L = \begin{cases} \frac{I_O}{1+\cos 2\pi D}\sin\left[\omega t + \pi\left(2D-\frac{2}{3}\right)\right] - I_O, & [0 \le \omega t \le 2\pi(1-D)] \\ \frac{I_O}{1+\cos 2\pi D} - I_O, & [2\pi(1-D) \le \omega t \le \pi] \\ \frac{I_O}{1+\cos 2\pi D}\sin\left[\omega t + \pi\left(2D-\frac{2}{3}\right)\right], & [\pi \le \omega t \le \pi(3-2D)] \\ -\frac{I_O}{1+\cos 2\pi D}, & [\pi(3-2D) \le \omega t \le 2\pi] \end{cases} \tag{11}$$

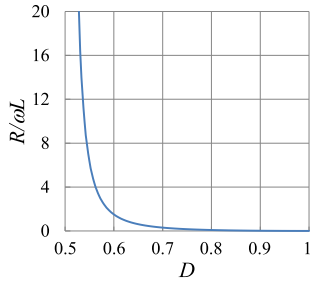

Fig. 3. $R/\omega L$ as a function of the diode-on-duty ratio D.

$$v_{D1} = \begin{cases} -\frac{\omega L I_O}{1+\cos 2\pi D}\cos\left[\omega t + \pi\left(2D-\frac{3}{2}\right)\right], & [0 \le \omega t \le 2\pi(1-D)] \\ 0, & [2\pi(1-D) \le \omega t \le \pi] \\ 0, & [\pi \le \omega t \le \pi(3-2D)] \\ 0, & [\pi(3-2D) \le \omega t \le 2\pi] \end{cases} \tag{12}$$

$$v_{D2} = \begin{cases} 0, & [0 \le \omega t \le 2\pi(1-D)] \\ 0, & [2\pi(1-D) \le \omega t \le \pi] \\ \frac{\omega L I_O}{1+\cos 2\pi D}\cos\left[\omega t + \pi\left(2D-\frac{3}{2}\right)\right], & [\pi \le \omega t \le \pi(3-2D)] \\ 0, & [\pi(3-2D) \le \omega t \le 2\pi] \end{cases} \tag{13}$$

$$v_L = \begin{cases} \frac{\omega L I_O}{1+\cos 2\pi D}\cos\left[\omega t + \pi\left(2D-\frac{3}{2}\right)\right], & [0 \le \omega t \le 2\pi(1-D)] \\ 0, & [2\pi(1-D) \le \omega t \le \pi] \\ \frac{\omega L I_O}{1+\cos 2\pi D}\cos\left[\omega t + \pi\left(2D-\frac{3}{2}\right)\right], & [\pi \le \omega t \le \pi(3-2D)] \\ 0, & [\pi(3-2D) \le \omega t \le 2\pi] \end{cases}. \tag{14}$$

V. Analysis for any Diode-on-Duty-Ratio

A. Component Value

The output voltage V_O is equal to the average of the diode voltage $-v_{D1}$

$$\begin{aligned} V_O = RI_O &= \frac{1}{2\pi}\int_0^{2\pi} -v_{D1}(\omega t)d(\omega t) \\ &= \frac{\omega L I_O(1-\cos 2\pi D)}{2\pi(1+\cos 2\pi D)}. \end{aligned} \tag{15}$$

From (15)

$$\frac{R}{\omega L} = \frac{1-\cos 2\pi D}{2\pi(1+\cos 2\pi D)}. \tag{16}$$

Fig. 3 shows $R/\omega L$ as a function of the diode-on-duty ratio D. As seen in Fig. 3, $R/\omega L$ increases from 0 to ∞ as D decreases from 1 to 0.5.

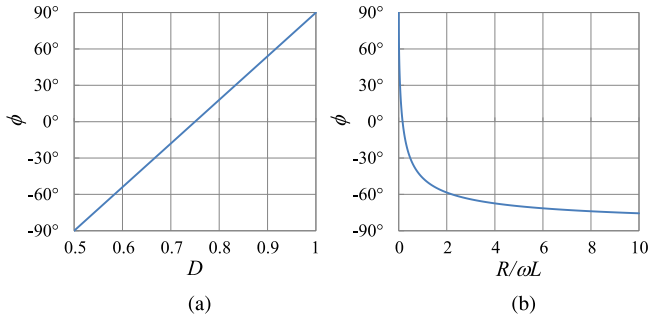

Fig. 4. Initial phase angle ϕ of the input current $i_{\rm IN}$ as a function of the diode-on-duty ratio D and that of $R/\omega L$. (a) $\phi - D$. (b) $\phi - R/\omega L$.

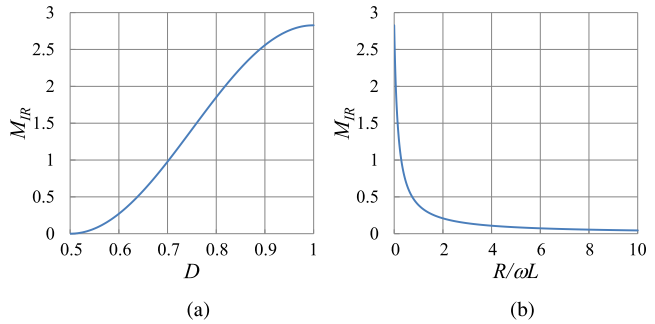

Fig. 5. Current transfer function M_{IR} as a function of the diode-on-duty ratio D and that of $R/\omega L$. (a) $M_{IR} - D$. (b) $M_{IR} - R/\omega L$.

B. Initial Phase Angle of the Input Current

In [40], the equation of the initial phase angle ϕ of the input current $i_{\rm IN}$ has been obtained

$$\phi = \pi\left(2D - \frac{2}{3}\right). \tag{17}$$

Fig. 4 shows the initial phase angle ϕ of the input current $i_{\rm IN}$ as a function of the diode-on-duty ratio D and that of $R/\omega L$. As seen in Fig. 4, ϕ decreases from 90° to −90° as D decreases from 1 to 0.5, or $R/\omega L$ increases from 0 to ∞.

C. Current Transfer Function

In [40], the equation of the output current I_O is given as

$$I_O = I_M(1 + \cos 2\pi D) \tag{18}$$

where I_M is the amplitude of the input current $i_{\rm IN}$.

From (18), the current transfer function M_{IR} is

$$M_{IR} = \frac{I_O}{I_{\rm RMS}} = \frac{I_O}{I_M/\sqrt{2}} = \sqrt{2}(1 + \cos 2\pi D) \tag{19}$$

where $I_{\rm RMS}$ is the RMS value of the input current $i_{\rm IN}$.

Fig. 5 shows the current transfer function M_{IR} as a function of the diode-on-duty ratio D and that of $R/\omega L$. As seen in Fig. 5, M_{IR} decreases from $2\sqrt{2}$ to 0 as D decreases from 1 to 0.5, or $R/\omega L$ increases from 0 to ∞. Moreover, the output current I_O is larger than the amplitude I_M of the input current $i_{\rm IN}$ at $D \geq 0.75$. In addition, the Class DE current driven low di/dt rectifier has low diode current stress. Thus, the Class DE current driven low di/dt rectifier is suitable for low voltage and large current power sources, such as the communication power supply, aircraft power supply, and electroplating power supply and so on [42].

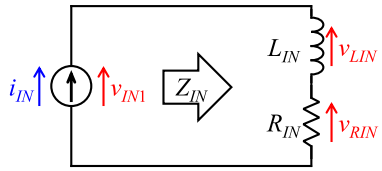

Fig. 6. Model of the input impedance $Z_{\rm IN}$ of the Class DE current driven low di/dt rectifier.

D. Normalized Input Impedance

The input power of the rectifier contains only the fundamental component because the input current $i_{\rm IN}$ is sinusoidal. Moreover, when the Class DE current driven low di/dt rectifier is implemented to a resonant dc/dc converter, the rectifier can be regarded as an input impedance $Z_{\rm IN}$. For this reason, it is sufficient to determine the input impedance $Z_{\rm IN}$ of the rectifier at the fundamental frequency f. Fig. 6 shows a model of the input impedance $Z_{\rm IN}$ of the Class DE current driven low di/dt rectifier. Because the rectifier is driven by the ac current source $i_{\rm IN}$, the input impedance $Z_{\rm IN}$ can be expressed as a series connection of the input resistor $R_{\rm IN}$ and the input inductor $L_{\rm IN}$.

From Fig. 1, the input voltage $v_{\rm IN}$ of the Class DE current driven low di/dt rectifier is equal to the inductor voltage v_L. The fundamental component $v_{\rm IN1}$ of the input voltage $v_{\rm IN}$ at the operating frequency f can be expressed as

$$\begin{aligned} v_{\rm IN1} &= v_{RIN} + v_{LIN} \\ &= V_{RIN}\sin(\omega t + \phi) + V_{LIN}\cos(\omega t + \phi) \end{aligned} \tag{20}$$

where v_{RIN} and v_{LIN} are the voltages across the input resister $R_{\rm IN}$ and the input inductor $L_{\rm IN}$, and V_{RIN} and V_{LIN} are the amplitudes of the voltages v_{RIN} and v_{LIN}, respectively.

The amplitudes V_{RIN} and V_{LIN} are calculated by the Fourier analysis as

$$\begin{aligned} V_{RIN} &= \frac{1}{\pi}\int_0^{2\pi} v_{\rm IN}\sin(\omega t + \phi)d(\omega t) \\ &= \frac{\omega L I_O}{\pi}(1 - \cos 2\pi D) \end{aligned} \tag{21}$$

$$\begin{aligned} V_{LIN} &= \frac{1}{\pi}\int_0^{2\pi} v_{\rm IN}\cos(\omega t + \phi)d(\omega t) \\ &= \frac{\omega L I_O}{\pi(1 + \cos 2\pi D)}\left[2\pi(1 - D) + \frac{1}{2}\sin 4\pi D\right] \end{aligned} \tag{22}$$

The input resistance $R_{\rm IN}$ can be obtained by dividing the amplitude V_{RIN} of the voltage v_{RIN} by the amplitude I_M of the input current $i_{\rm IN}$. From (18) and (21), the input resistance $R_{\rm IN}$ is

$$R_{\rm IN} = \frac{V_{RIN}}{I_M} = \frac{\omega L}{\pi}(1 - \cos 2\pi D)(1 + \cos 2\pi D). \tag{23}$$

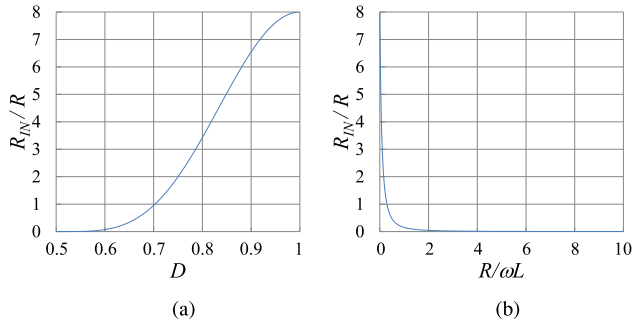

Fig. 7. Normalized input resistance $R_{\rm IN}/R$ as a function of the diode-on-duty ratio D and that of $R/\omega L$. (a) $R_{\rm IN}/R - D$. (b) $R_{\rm IN}/R - R/\omega L$.

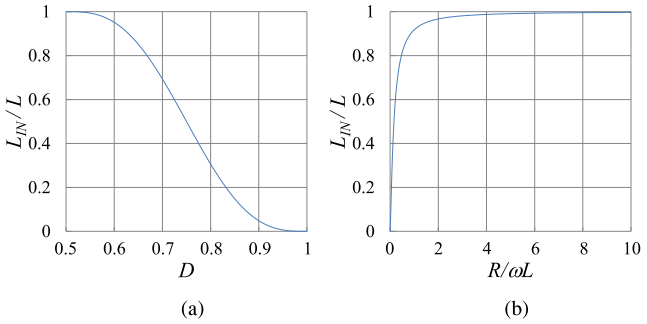

Fig. 8. Normalized input inductance $L_{\rm IN}/L$ as a function of the diode-on-duty ratio D and that of $R/\omega L$. (a) $L_{\rm IN}/L - D$. (b) $L_{\rm IN}/L - R/\omega L$.

Therefore, from (16) and (23), the normalized input resistance $R_{\rm IN}/R$ is

$$\frac{R_{\rm IN}}{R} = 2(1+\cos 2\pi D)^2. \tag{24}$$

Similarly, the input reactance $\omega L_{\rm IN}$ can be obtained by dividing the amplitude V_{LIN} of the voltage v_{LIN} by the amplitude I_M of the input current $i_{\rm IN}$. From (18) and (22), the input reactance $\omega L_{\rm IN}$ is

$$\omega L_{\rm IN} = \frac{V_{LIN}}{I_M} = \frac{\omega L}{\pi}\left[2\pi(1-D)+\frac{1}{2}\sin 4\pi D\right]. \tag{25}$$

Thus, the normalized input inductance $L_{\rm IN}/L$ is

$$\frac{L_{\rm IN}}{L} = \frac{1}{\pi}\left[2\pi(1-D)+\frac{1}{2}\sin 4\pi D\right]. \tag{26}$$

Fig. 7 shows the normalized input resistance $R_{\rm IN}/R$ as a function of the diode-on-duty ratio D and that of $R/\omega L$. As seen in Fig. 7, $R_{\rm IN}/R$ decreases from 8 to 0 as D decreases from 1 to 0.5, or $R/\omega L$ increases from 0 to ∞.

Fig. 8 shows the normalized input inductance $L_{\rm IN}/L$ as a function of the diode-on-duty ratio D and that of $R/\omega L$. As seen in Fig. 8, $L_{\rm IN}/L$ increases from 0 to 1 as D decreases from 1 to 0.5, or $R/\omega L$ increases from 0 to ∞.

The normalized input resistance $R_{\rm IN}/\omega L$ is obtained from (23)

$$\frac{R_{\rm IN}}{\omega L} = \left(\frac{R_{\rm IN}}{R}\right)\left(\frac{R}{\omega L}\right) = \frac{1}{\pi}(1-\cos 2\pi D)(1+\cos 2\pi D). \tag{27}$$

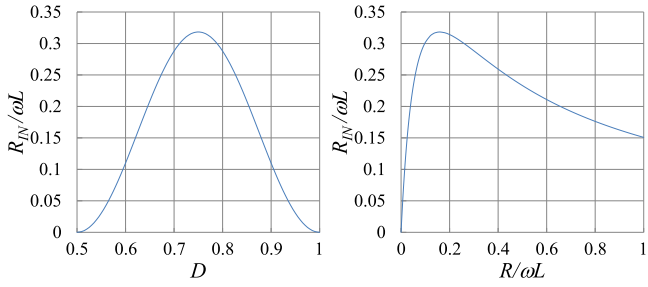

Fig. 9. Normalized input resistance $R_{\rm IN}/\omega L$ as a function of the diode-on-duty ratio D and that of $R/\omega L$. (a) $R_{\rm IN}/\omega L - D$. (b) $R_{\rm IN}/\omega L - R/\omega L$.

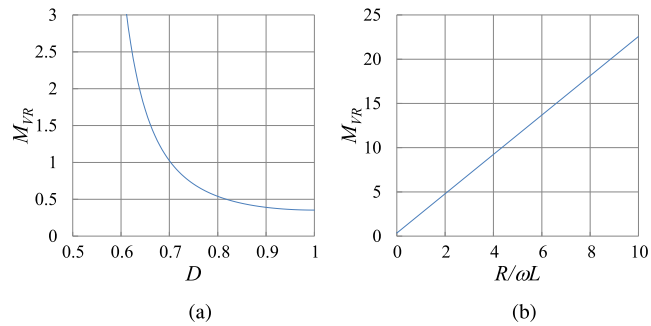

Fig. 10. Voltage transfer function $M_{V\,R}$ as a function of the diode-on-duty ratio D and that of $R/\omega L$. (a) $M_{V\,R} - D$. (b) $M_{V\,R} - R/\omega L$.

Fig. 9 shows the normalized input resistance $R_{\rm IN}/\omega L$ as a function of the diode-on-duty ratio D and that of $R/\omega L$. The maximum value of $R_{\rm IN}/\omega L$ is 0.3183 and occurs at $D = 0.75$ or $R/\omega L = 0.1592$. For $D > 0.75$ or $R/\omega L > 0.1592$, $R_{\rm IN}/\omega L$ decreases as $R/\omega L$ increases. Thus, the rectifier acts as an impedance inverter. Therefore, it is compatible with a Class E inverter [43], in which the switch turns on at ZVS only for load resistance ranging from 0 to a maximum value [27], [44]–[47].

E. Voltage Transfer Function

The input power $P_{\rm IN}$ of the rectifier is

$$P_{\rm IN} = \frac{V_{\rm IN1RMS}^2}{R_{\rm IN}} \tag{28}$$

where $V_{\rm IN1RMS}$ is the RMS value of the fundamental component $v_{\rm IN1}$ of the input voltage $v_{\rm IN}$. Assuming that the efficiency of the rectifier is 100%, the input power $P_{\rm IN}$ is equal to the output power $P_{\rm OUT}$

$$P_{\rm IN} = P_{\rm OUT} \Longleftrightarrow \frac{V_{\rm IN1RMS}^2}{R_{\rm IN}} = \frac{{V_O}^2}{R}. \tag{29}$$

Thus, from (24) and (29), the voltage transfer function $M_{V\,R}$ is

$$M_{V\,R} = \frac{V_O}{V_{\rm IN1RMS}} = \sqrt{\frac{R}{R_{\rm IN}}} = \frac{1}{\sqrt{2}(1+\cos 2\pi D)}. \tag{30}$$

Fig. 10 shows the voltage transfer function $M_{V\,R}$ as a function of the diode-on-duty ratio D and that of $R/\omega L$. As seen in

Fig. 10, M_{VR} increases from $1/\sqrt{2}$ to ∞ as D decreases from 1 to 0.5, or $R/\omega L$ increases from 0 to ∞.

F. Diode Voltage Stress

To determine the peak value V_{DM} of the diode reverse voltages v_{D1} and v_{D2}, two cases must be considered.

In the case of $D < 0.75$, differentiating (12)

$$\frac{dv_{D1}}{d(\omega t)} = -\frac{\omega L I_O}{1+\cos 2\pi D}\sin\left[\omega t + \pi\left(2D-\frac{3}{2}\right)\right]. \quad (31)$$

Setting $dv_{D1}/d(\omega t)$ to 0, the phase which the peak value V_{DM1} of the diode reverse voltage v_{D1} occurs can be obtained

$$\omega t = -\phi. \quad (32)$$

Similarly, differentiating (13)

$$\frac{dv_{D2}}{d(\omega t)} = -\frac{\omega L I_O}{1+\cos 2\pi D}\sin\left[\omega t + \pi\left(2D-\frac{3}{2}\right)\right]. \quad (33)$$

Setting $dv_{D2}/d(\omega t)$ to 0, the phase which the peak value V_{DM2} of the diode reverse voltage v_{D2} occurs can be obtained

$$\omega t = \pi - \phi. \quad (34)$$

Hence, from (12) and (13), the peak value V_{DM} of the diode reverse voltages v_{D1} and v_{D2} is

$$\begin{aligned} V_{DM} &= V_{DM1} = V_{DM2} \\ &= v_{D1}(-\phi) = v_{D2}(\pi-\phi) \\ &= \frac{\omega L I_O}{1+\cos 2\pi D}, \qquad [0.5 < D < 0.75]. \end{aligned} \quad (35)$$

On the other hand, in the case of $D \geq 0.75$, the peak value V_{DM1} of the diode reverse voltage v_{D1} occurs when the diode D_1 turns off

$$\omega t = 0. \quad (36)$$

Similarly, the peak value V_{DM2} of the diode reverse voltage v_{D2} occurs when the diode D_2 turns off

$$\omega t = \pi. \quad (37)$$

Hence, from (12) and (13), the peak value V_{DM} of the diode reverse voltages v_{D1} and v_{D2} is

$$\begin{aligned} V_{DM} &= V_{DM1} = V_{DM2} \\ &= v_{D1}(0) = v_{D2}(\pi) \\ &= -\frac{\omega L I_O}{1+\cos 2\pi D}\sin 2\pi D, \quad [D \geq 0.75]. \end{aligned} \quad (38)$$

Therefore, from (15), (16), (35), and (38), the normalized diode voltage stress V_{DM}/V_O is

$$\frac{V_{DM}}{V_O} = \begin{cases} \dfrac{2\pi}{1-\cos 2\pi D}, & [0.5 < D < 0.75] \\ -\dfrac{2\pi}{1-\cos 2\pi D}\sin 2\pi D, & [D \geq 0.75]. \end{cases} \quad (39)$$

Fig. 11 shows the normalized diode voltage stress V_{DM}/V_O as a function of the diode-on-duty ratio D and that of $R/\omega L$. As seen in Fig. 11, V_{DM}/V_O increases from π to ∞ as D increases from 0.5 to 1, or $R/\omega L$ decreases from ∞ to 0.

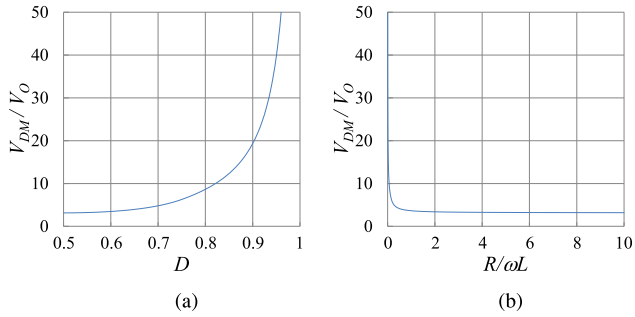

Fig. 11. Normalized diode voltage stress V_{DM}/V_O as a function of the diode-on-duty ratio D and that of $R/\omega L$. (a) V_{DM}/V_O –D. (b) V_{DM}/V_O – $R/\omega L$.

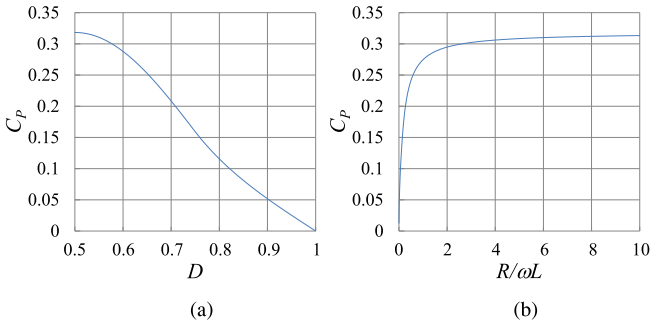

Fig. 12. Power-output capability C_P as a function of the diode-on-duty ratio D and that of $R/\omega L$. (a) C_P –D. (b) C_P – $R/\omega L$.

G. Power-Output Capability

The power-output capability can be used to compare the circuits in the aspect of the effective usage of the semiconductor switches. From (9) and (10), the peak value I_{DM} of the diode currents i_{D1} and i_{D2} is

$$I_{DM} = I_O. \quad (40)$$

Thus, from (39) and (40), the power-output capability C_P is

$$C_P = \frac{P_O}{I_{DM}V_{DM}} = \begin{cases} \dfrac{1-\cos 2\pi D}{2\pi}, & [0.5 < D < 0.75] \\ -\dfrac{1-\cos 2\pi D}{2\pi \sin 2\pi D}, & [D \geq 0.75]. \end{cases} \quad (41)$$

Fig. 12 shows the power-output capability C_P as a function of the diode-on-duty ratio D and that of $R/\omega L$. As seen in Fig. 12, C_P decreases from $1/\pi$ to 0 as D increases from 0.5 to 1, or $R/\omega L$ decreases from ∞ to 0.

VI. Power Conversion Efficiency

The power conversion efficiency of the Class DE current driven low di/dt rectifier can be defined as

$$\eta = \frac{P_O}{P_O + P_D + P_L + P_{LF}} \quad (42)$$

where P_D is the power loss at the diodes D_1 and D_2, P_L is the power loss at the inductor L, and P_{LF} is the power loss at the filter inductor L_F.

The power loss at the diodes D_1 and D_2 is

$$P_D = P_{D1} + P_{D2} \tag{43}$$

where P_{D1} and P_{D2} are the power loss at the diodes D_1 and D_2, respectively.

The power loss at the each diode can be expressed as

$$P_{D1} = I_{D1AVE} \cdot V_{F1} + R_{\rm ON1} \cdot I^2_{D1\rm RMS} \tag{44}$$

$$P_{D2} = I_{D2AVE} \cdot V_{F2} + R_{\rm ON2} \cdot I^2_{D2\rm RMS} \tag{45}$$

where I_{D1AVE} and I_{D2AVE} are the averaged values of the diode currents i_{D1} and i_{D2}, V_{F1} and V_{F2} are the forward voltage drops of the diodes D_1 and D_2, $R_{\rm ON1}$ and $R_{\rm ON2}$ are the ON resistances of the diodes D_1 and D_2, and $I_{D1\rm RMS}$ and $I_{D2\rm RMS}$ are the RMS values of the diode currents i_{D1} and i_{D2}, respectively.

From (9) and (10), the averaged values I_{D1AVE} and I_{D2AVE} of the diode currents i_{D1} and i_{D2} are expressed as

$$I_{D1AVE} = \frac{1}{2\pi}\int_0^{2\pi} i_{D1}\, d(\omega t) = \frac{I_O}{2} \tag{46}$$

$$I_{D2AVE} = \frac{1}{2\pi}\int_0^{2\pi} i_{D2}\, d(\omega t) = \frac{I_O}{2}. \tag{47}$$

The RMS values $I_{D1\rm RMS}$ and $I_{D2\rm RMS}$ of the diode currents i_{D1} and i_{D2} are also from (9) and (10)

$$I_{D1\rm RMS} = \left[\frac{1}{2\pi}\int_0^{2\pi} i^2_{D1}\, d(\omega t)\right]^{\frac{1}{2}} = \frac{I_O}{\sqrt{2\pi}}\Big[\left(\frac{1}{1+\cos 2\pi D}\right)^2 \times \left(\frac{1}{2}\sin 4\pi D + 4\sin 2\pi D + 6\pi D - 3\pi\right) - \frac{2}{1+\cos 2\pi D}(\sin 2\pi D + 2\pi D - \pi) + \pi\Big]^{\frac{1}{2}} \tag{48}$$

$$I_{D2\rm RMS} = \left[\frac{1}{2\pi}\int_0^{2\pi} i^2_{D2}\, d(\omega t)\right]^{\frac{1}{2}} = \frac{I_O}{\sqrt{2\pi}}\Big[\left(\frac{1}{1+\cos 2\pi D}\right)^2 \times \left(\frac{1}{2}\sin 4\pi D + 4\sin 2\pi D + 6\pi D - 3\pi\right) - \frac{2}{1+\cos 2\pi D}(\sin 2\pi D + 2\pi D - \pi) + \pi\Big]^{\frac{1}{2}}. \tag{49}$$

From (43)–(49), the power loss at the diodes D_1 and D_2 can be obtained

$$P_D = \frac{I_O}{2}\cdot(V_{F1}+V_{F2}) + (R_{\rm ON1}+R_{\rm ON2})\cdot \frac{I_O^2}{2\pi}\Big[\left(\frac{1}{1+\cos 2\pi D}\right)^2\left(\frac{1}{2}\sin 4\pi D + 4\sin 2\pi D + 6\pi D - 3\pi\right) - \frac{2}{1+\cos 2\pi D}(\sin 2\pi D + 2\pi D - \pi) + \pi\Big]. \tag{50}$$

The power loss at the inductor L can be expressed as

$$P_L = R_L \cdot I^2_{L\rm RMS} \tag{51}$$

where R_L is the ESR of the inductor L, $I_{L\rm RMS}$ is the RMS value of the inductor current i_L.

From (11), the RMS value of the inductor current i_L is expressed as

$$I_{L\rm RMS} = \left[\frac{1}{2\pi}\int_0^{2\pi} i_L^2\, d(\omega t)\right]^{\frac{1}{2}} = \frac{I_O}{\sqrt{2\pi}}\left[\frac{1}{2}\left(\frac{1}{1+\cos 2\pi D}\right)^2(4\pi D - \sin 4\pi D) + \frac{2}{1+\cos 2\pi D}(\sin 2\pi D - 2\pi D + \pi) + \pi\right]^{\frac{1}{2}}. \tag{52}$$

Thus, from (51) and (52), the power loss at the inductor L can be obtained

$$P_L = R_L \cdot \frac{I_O^2}{2\pi}\Big[\frac{1}{2}\left(\frac{1}{1+\cos 2\pi D}\right)^2(4\pi D - \sin 4\pi D) + \frac{2}{1+\cos 2\pi D}(\sin 2\pi D - 2\pi D + \pi) + \pi\Big]. \tag{53}$$

Assuming that the filter inductance L_F is large enough to feed a constant current I_O, the power loss at the filter inductor L_F can be expressed as

$$P_{LF} = R_{LF} \cdot I_O^2 \tag{54}$$

where R_{LF} is the ESR of the filter inductor L_F.

Substituting (50), (53), and (54) into (42), the power conversion efficiency of the Class DE current driven low di/dt rectifier is obtained.

VII. Circuit Design Method

A Class DE current driven low di/dt rectifier is designed on the following specifications:

1) the operating frequency $f = 200$ kHz, where $f = \omega/2\pi$;
2) the output voltage $V_O = 5.00$ V;
3) the output power $P_O = 1.25$ W;
4) the diode-on-duty-ratio $D = 0.75$.

From specifications, the load resistance R is

$$R = \frac{V_O^2}{P_O} = \frac{5.00^2}{1.25} = 20.0\ \Omega. \tag{55}$$

The output current I_O is

$$I_O = \frac{P_O}{V_O} = \frac{5.00}{1.25} = 0.250\ \text{A}. \tag{56}$$

Thus, from (18) and (56), the amplitude I_M of the input current $i_{\rm IN}$ is

$$I_M = \frac{I_O}{1+\cos 2\pi D} = \frac{0.250}{1+\cos(2\pi\cdot 0.750)} = 0.25\ \text{A}. \tag{57}$$

From (16) and (55), the inductance L is

$$L = \frac{2\pi R(1+\cos 2\pi D)}{\omega(1-\cos 2\pi D)} = \frac{2\pi\cdot 20.0[1+\cos(2\pi\cdot 0.750)]}{2\pi\cdot 200\cdot 10^3[1-\cos(2\pi\cdot 0.750)]} = 100\,\mu\text{H}. \tag{58}$$

The cutoff frequency f_C in the second-order low-pass filter is designed at 700 Hz. Giving the filter inductor $L_F = 1.00$ mH,

TABLE II
DESIGNED AND MEASURED VALUE OF THE CIRCUIT COMPONENTS

Components		Designed	Measured	(ESR[Ω])
Inductance L	[μH]	100	100	(0.052)
Filter inductance L_F	[mH]	1.00	1.06	(0.076)
Filter capacitance C_F	[μF]	51.7	51.7	(2.44)
Load resistance R	[Ω]	20.0	20.0	–
Diode junction capacitance C_J	[pF]	0	5*	–
Diode forward voltage drop V_F	[V]	0	0.7*	–
Diode-on resistance V_F	[Ω]	0	0.31*	–

*Obtained from the datasheet of the diode ERA91-021 [48].

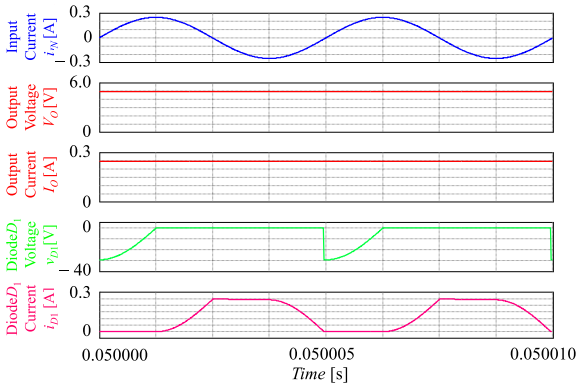

Fig. 13. Simulation waveforms in the rectifier of Fig. 1 in the case of designed values in Table II.

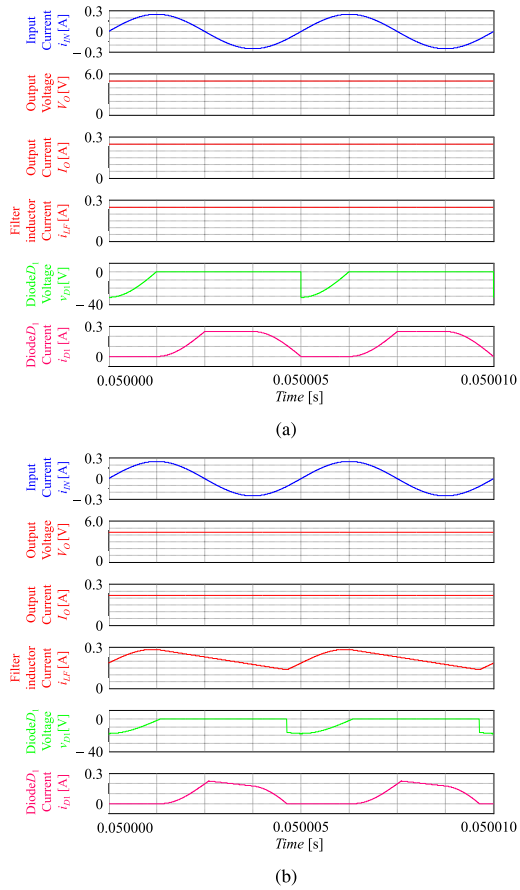

Fig. 14. Simulation waveforms in the rectifier of Fig. 1 in the case of large filter inductance ($L_F = 10$ mH) and small filter inductance ($L_F = 0.1$ mH). (a) In the case of large filter inductance ($L_F = 10$ mH). (b) In the case of small filter inductance ($L_F = 0.1$ mH).

the filter capacitance C_F is

$$C_F = \frac{1}{4\cdot\pi^2\cdot f_C^2\cdot L_F} = \frac{1}{4\cdot\pi^2\cdot 700^2\cdot 1.00} = 51.7\ \mu\text{F}. \quad (59)$$

Table II shows the designed values and the measured values of the circuit components.

VIII. SIMULATION RESULTS

To verify the accuracy of the circuit design method and waveforms of Fig. 2, the Class DE current driven low di/dt rectifier was simulated with PSIM version 9.1. In the simulation, the ideal ac current source model, in which the amplitude and the operating frequency can be set to required values, was used as the input current source for the rectifier. The component values of the rectifier were the designed values in Table II. Fig. 13 shows the simulation waveforms. As seen in Fig. 13, the diode D_1 turns on at ZCS, ZCDS, ZVS, and low dv/dt, and turns off at ZCS and low di/dt. Moreover, the diode current stress of the rectifier is no more than the output current I_O. The measured values of the output voltage V_O was 4.92 V. The diode-on-duty ratio was 0.739, which was measured in Fig. 13. The output voltage and the diode-on-duty ratio had differences between the designed values and the simulation results. These differences could be caused by the component value of the filter inductor L_F.

Fig. 14 shows the simulation waveforms in the case of large filter inductance ($L_F = 10$ mH) and small filter inductance

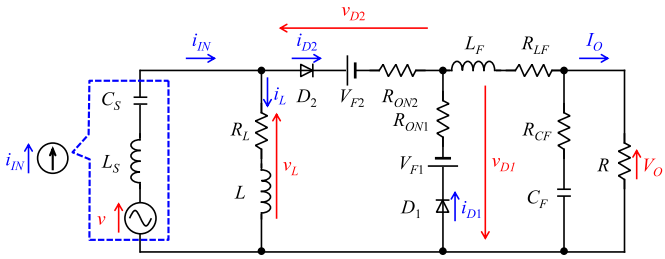

Fig. 15. Experimental circuit of the Class DE current driven low di/dt rectifier.

($L_F = 0.1$ mH). As seen in Figs. 13 and 14, the filter inductance is larger, the output voltage and the diode-on-duty ratio is getting closer 5.00 and 0.750 V, respectively. Moreover, when the inductance value of the filter inductor L_F is small, a current ripple is large for the current i_{LF} through the filter inductor L_F. The current i_{LF} through the filter inductor L_F is the sum of the diodefs current i_{D1} and i_{D2}. Thus, in the case of large filter inductance ($L_F = 10$ mH), the maximum value of the current i_{D1} through the diode D_1 is flat due to small current ripple. On the other hand, in the case of small filter inductance ($L_F = 0.1$mH),

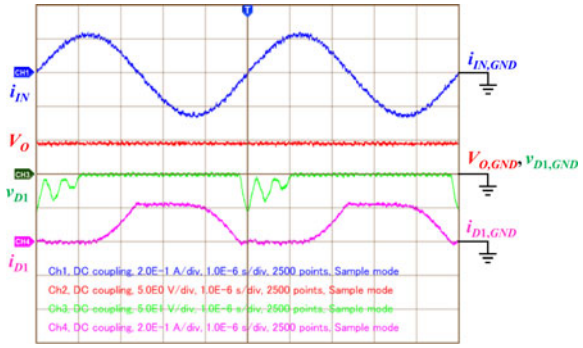

Fig. 16. Observed waveforms in the Class DE current driven low di/dt rectifier against fundamental component. $i_{\rm IN}$: 0.20 A/div; V_O: 5.0 V/div; v_{D1}: 50.0 V/div; i_{D1}: 0.20 A/div, horizontal: 1 μs.

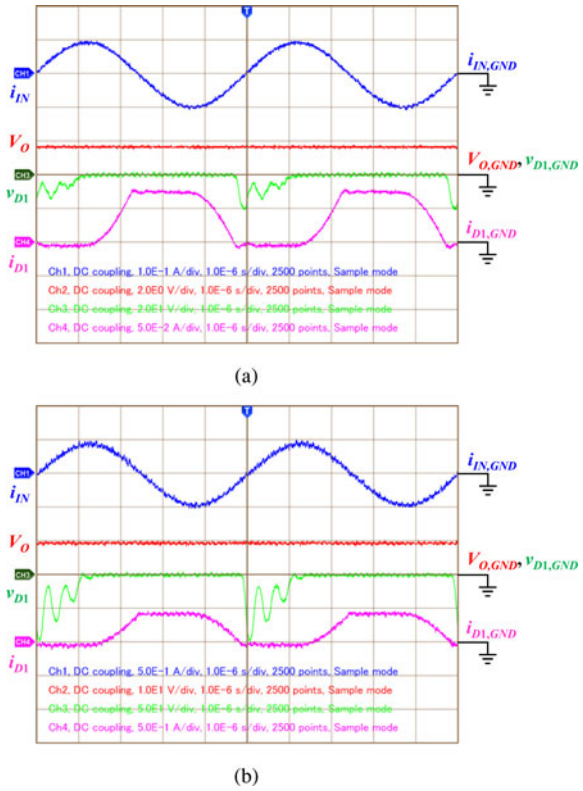

Fig. 17. Observed waveforms in the Class DE current driven low di/dt rectifier against input current variation. (a) $I_M = 0.1$ A. $i_{\rm IN}$: 0.10 A/div; V_O: 2.0 V/div; v_{D1}: 20 V/div; i_{D1}: 0.05 A/div, horizontal: 1 μs. (b) $I_M = 0.5$ A. $i_{\rm IN}$: 0.50 A/div; V_O: 10 V/div; v_{D1}: 50 V/div; i_{D1}: 0.50 A/div, horizontal: 1 μs.

the maximum value of the current i_{D1} through the diode D_1 is not flat due to large current ripple.

IX. Experimental Results

A. Fundamental Operation

The Class DE current driven low di/dt rectifier shown in Fig. 1 was built and experimented at the fundamental operation. Fig. 15 shows the experimental circuit of the Class DE current driven low di/dt rectifier, where the ESR R_L of the inductor

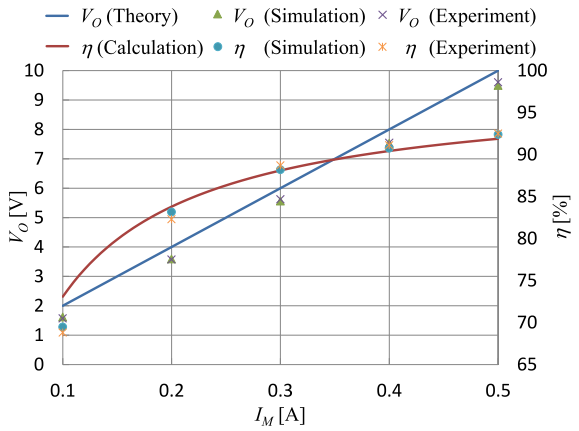

Fig. 18. Characteristic of the power conversion efficiency η and the output voltage V_O against input current variation.

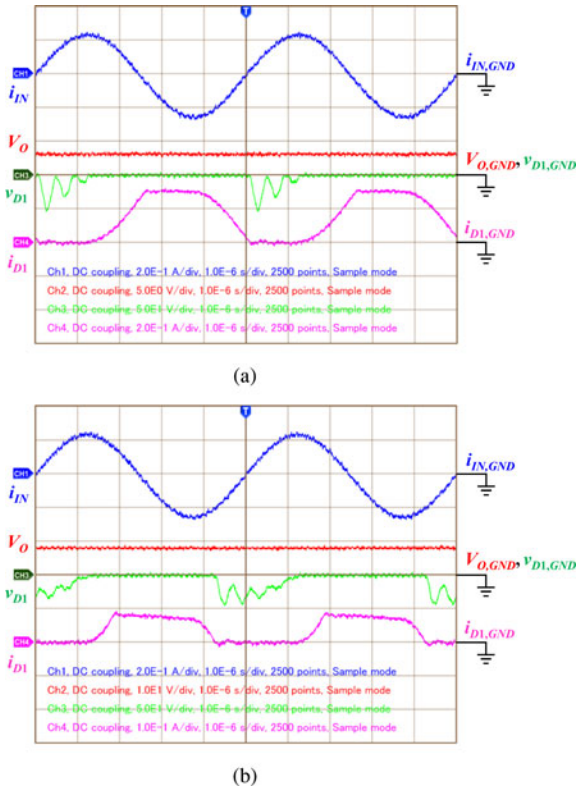

Fig. 19. Observed waveforms in the Class DE current driven low di/dt rectifier against load resistance variation. (a) $R = 10\ \Omega$. $i_{\rm IN}$: 0.20 A/div; V_O: 5.0 V/div; v_{D1}: 50 V/div; i_{D1}: 0.20 A/div, horizontal: 1 μs. (b) $R = 100\ \Omega$. $i_{\rm IN}$: 0.20 A/div; V_O: 10 V/div; v_{D1}:50 V/div; i_{D1}: 0.10 A/div, horizontal: 1 μs.

L, the diode-on resistances $R_{\rm ON1}$ and $R_{\rm ON2}$, the diode forward voltage drops V_{F1} and V_{F2}, the ESR R_{LF} of the filter inductor, and the ESR R_{CF} of the filter capacitor were considered. The measured values of the circuit components are shown in Table II. The experimental method in [15]–[18], [39] was adopted to compose an approximate ideal ac current source. The approximate ideal ac current source was composed of a function generator (Tektronix AFG3011), a bipolar power source

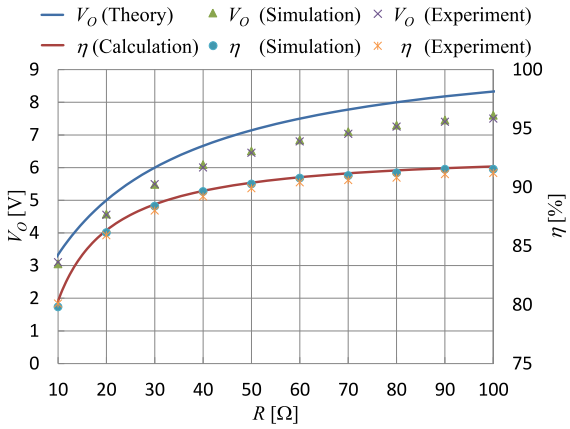

Fig. 20. Characteristic of the power conversion efficiency η and the output voltage V_O against load resistance variation.

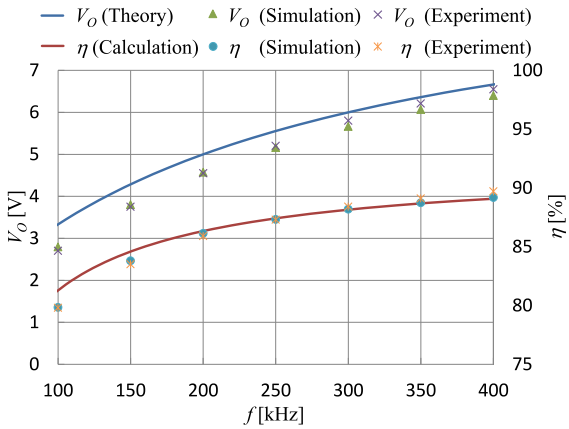

Fig. 22. Characteristic of the power conversion efficiency η and the output voltage V_O against operating frequency variation.

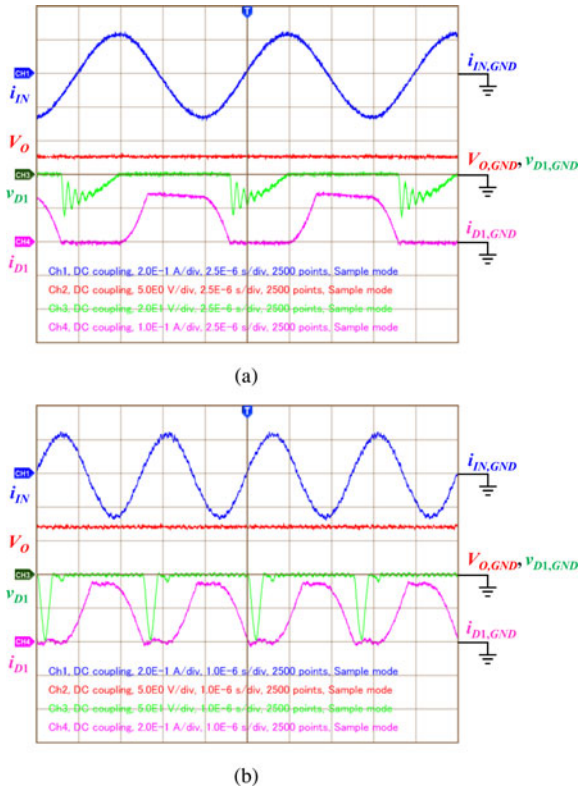

Fig. 21. Observed waveforms in the Class DE current driven low di/dt rectifier against operating frequency variation. (a) $f = 100$ kHz. $i_{\rm IN}$: 0.20 A/div; V_O: 5.0 V/div; v_{D1}: 20 V/div; i_{D1}: 0.10 A/div, horizontal: 2.5 μs. (b) $f = 400$ kHz. $i_{\rm IN}$: 0.20 A/div; V_O:5.0 V/div; v_{D1}: 50 V/div; i_{D1}: 0.20 A/div, horizontal: 1 μs.

(NF HSA4011), and a series resonant circuit L_S and C_S, which was designed at high Q value. The input current $i_{\rm IN}$ and the diode current i_{D1} were observed by means of the current probes (Tektronix TCPA300). Fig. 16 shows the observed waveforms of the input current $i_{\rm IN}$, the output voltage V_O, the diode reverse voltage v_{D1}, and the diode current i_{D1}. The measured values of the output voltage V_O was 4.55 V. The output voltage was lower than the simulation results due to the ESRs of the components, and the diode forward voltage drops V_{F1} and V_{F2} and the diode-on resistances $R_{\rm ON1}$ and $R_{\rm ON2}$. The measured power conversion efficiency was 85.9%.

As seen in Fig. 16, the diodes D_1 turned on at ZCS, ZCDS, ZVS, and low dv/dt, and turned off at ZCS and low di/dt. The obtained diode current waveform i_{D1} was corresponded with the idealized diode current waveform. However, the diode voltage waveform v_{D1} had ringing. The resonance was caused by the junction capacitance C_J of the diode D_1 and the inductor L. The measured resonant frequency of the diode voltage waveform v_{D1} was 2.38 MHz. On the other hand, the calculated resonant frequency of the diode voltage waveform v_{D1} was 7.12 MHz. The difference between the measured resonant frequency and the calculated resonant frequency could be caused by: 1) the nonlinearity of the junction capacitance C_J, 2) Equivalent series inductance of the circuit, and 3) the earth capacity of the probe and the input capacity of the oscilloscope, because the probe connects the diode D_1 in order to obtain the diode voltage waveform v_{D1}.

B. Characteristic Against Input Current Variation

The characteristic of the output voltage V_O and the power conversion efficiency η were obtained when the amplitude I_M of the input current $i_{\rm IN}$ varied from 0.1 to 0.5 A. The other experimental conditions were fixed at the measured values in Table II. Fig. 17 shows the experimental results at $I_M = 0.1$ A and $I_M = 0.5$ A. As seen in Fig. 17, even if the amplitude I_M of the input current $i_{\rm IN}$ varied, the diodes D_1 turned on at ZCS, ZCDS, ZVS, and low dv/dt, and turned off at ZCS and low di/dt. Fig. 18 shows the characteristic of the output voltage V_O and the power conversion efficiency η as functions of the amplitude I_M of the input current $i_{\rm IN}$. The theoretical output voltage V_O and the calculation of the power conversion efficiency η were obtained by (15) and (42), respectively. As seen in Fig. 18, the output voltage V_O seems to be proportional to the amplitude I_M of the input current $i_{\rm IN}$. The higher output voltage V_O offers the higher power conversion efficiency η.

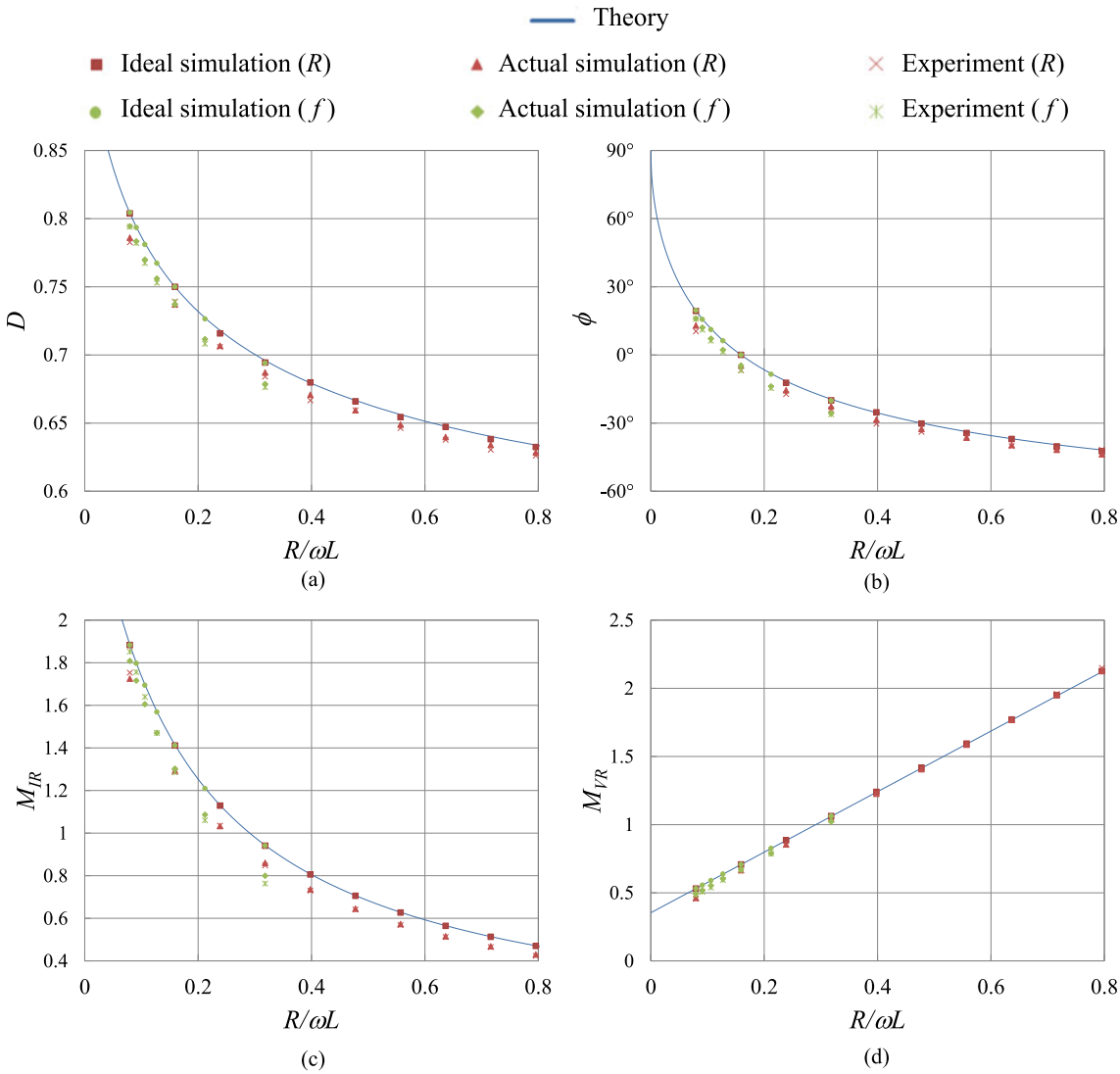

Fig. 23. Relationship between the derivations, simulation results, and experimental results. (a) $D - R/\omega L$. (b) $\phi - R/\omega L$. (c) $M_{IR} - R/\omega L$. (d) $M_{VR} - R/\omega L$.

C. Characteristic Against Load Resistance Variation

The characteristic of the output voltage V_O and the power conversion efficiency η were obtained when the load resistance R varied from 10 to 100 Ω. The other experimental conditions were fixed at the measured values in Table II. Fig. 19 shows the experimental results at $R = 10$ Ω and $R = 100$ Ω. As seen in Fig. 19, even if the load resistance R varied, the diodes D_1 turned on at ZCS, ZCDS, ZVS, and low dv/dt, and turned off at ZCS and low di/dt. Fig. 20 shows the characteristic of the output voltage V_O and the power conversion efficiency η as functions of the load resistance R. The theoretical output voltage V_O and the calculation of the power conversion efficiency η were obtained by (15) and (42), respectively. As seen in Fig. 20, the output voltage V_O and the power conversion efficiency η were getting higher when the load resistance R increased.

D. Characteristic Against Operating Frequency Variation

The characteristic of the output voltage V_O and the power conversion efficiency η were obtained when the operating frequency f varied from 100 to 400 kHz. The other experimental conditions were fixed at the measured valued in Table II. Fig. 21 shows the experimental results at $f = 100$ kHz and $f = 400$ kHz. As seen in Fig. 21, even if the operating frequency f varied, the diodes D_1 turned on at ZCS, ZCDS, ZVS, and low dv/dt, and turned off at ZCS and low di/dt. Fig. 22 shows the characteristic of the output voltage V_O and the power conversion efficiency η as functions of the operating frequency f. The theoretical output voltage V_O and the calculation of the power conversion efficiency η were obtained by (15) and (42), respectively. As seen in Fig. 22, the output voltage V_O and the power conversion efficiency η increased when the operating frequency f increased.

X. Relationship Between the Equations, Simulation Results, and Experimental Results

Fig. 23 shows the relationship between the equations, simulation results, and experimental results, where "Theory" shows the same curves to those shown in Figs. 3, 4(b), 5(b), and 10(b), "Ideal simulation (R)" is the simulation results in an ideal condition, "Actual simulation (R)" is the simulation results in the case of using the measured values in Table II, "Experiment (R)" is the experimental results when the load resistance R varied from 10 to 100 Ω, "Ideal simulation (f)" is the simulation results in an ideal condition, "Actual simulation (f)" is the simulation results in the case of using the measured values in Table II, "Experiment (f)" is the experimental results when the operating frequency f varied from 100 to 400 kHz. As seen in Fig. 23, "Theory," "Ideal simulation (R)," and "Ideal simulation (f)" are in good agreement. Moreover, "Actual simulation (R)," "Experiment (R)," "Actual simulation (f)," and "Experiment (f)" are lower than "Theory" due to the ESRs of the components, the diode forward voltage drops V_{F1} and V_{F2}, and the diode-on resistances $R_{\mathrm{ON}1}$ and $R_{\mathrm{ON}2}$.

XI. Conclusion

The analysis of the Class DE current driven low di/dt rectifier for any diode-on-duty ratio has been carried out. The initial phase angle of the input current, the current and voltage transfer function, the normalized input resistance and inductance, the normalized diode voltage stress, and the power-output capability have been obtained and clarified as functions of the diode-on-duty ratio and those of R/wL. Moreover. the power conversion efficiency and the circuit design have been shown. The performance of the Class DE current driven low di/dt rectifier has been confirmed with the circuit simulations and the experiments. In the experiment and the simulation, the characteristics of the output voltage and the power conversion efficiency against the amplitude of the input current, the operating frequency, and the load resistance have been obtained. In addition, the relationship between the equations, simulation results, and experimental results have been obtained. Theoretical, simulation, and experimental results were in good agreement.

References

[1] M. Mikotajewski, "Class D synchronous rectifiers," *IEEE Trans. Circuits Syst.*, vol. 38, no. 7, pp. 694–697, Jul. 1991.

[2] M. K. Kazimierczuk, "Class D current-driven rectifiers for resonant dc/dc converter applications," *IEEE Trans. Ind. Electron.*, vol. 38, no. 5, pp. 344–354, Oct. 1991.

[3] M. K. Kazimierczuk, M. J. Mescher, and R. M. Prenger, "Class D current-driven transformer center-tapped controllable synchronous rectifier," *IEEE Trans. Circuits Syst. I, Fundam. Theory Appl.*, vol. 43, no. 8, pp. 670–680, Aug. 1996.

[4] M. K. Kazimierczuk, W. Szaraniec, and S. Wang, "Analysis and design of parallel resonant converter at high Q_L," *IEEE Trans. Aerosp. Electron. Syst.*, vol. 28, no. 1, pp. 35–50, Jan. 1992.

[5] M. K. Kazimierczuk and J. Jóźwik, "Class E zero-voltage-switching and zero-current-switching rectifiers," *IEEE Trans. Circuits Syst.*, vol. 37, no. 3, pp. 436–444, Mar. 1990.

[6] A. Reatti and M. K. Kazimierczuk, "Comparison of the efficiencies of class D and class E rectifiers," in *Proc. 36th Midwest Symp. Circuits Syst.*, Aug. 1993, pp. 871–874.

[7] M. K. Kazimierczuk, "Class E low dv_D/dt rectifier," *Proc. IEE*, vol. 136, no. 6 Pt. B, pp. 257–262, Nov. 1989.

[8] M. K. Kazimierczuk and J. Jóźwik, "Resonant dc/dc converter with class-E inverter and class-E rectifier," *IEEE Trans. Ind. Electron.*, vol. 36, no. 4, pp. 568–578, Nov. 1989.

[9] M. K. Kazimierczuk, "Analysis of class E zero-voltage-switching rectifier," *IEEE Trans. Circuits Syst.*, vol. 37, no. 6, pp. 747–755, Jun. 1990.

[10] A. Reatti, M. K. Kazimierczuk, and R. Redl, "Class E full-wave low dv/dt rectifier," *IEEE Trans. Circuits Syst.*, vol. 40, no. 2, pp. 73–84, Feb. 1993.

[11] A. Reatti and M. K. Kazimierczuk, "Efficiency of the transformer version of class E half-wave low dv_D/dt rectifier," in *Proc. 36th Midwest Symp. Circuits Syst.*, Aug. 1993, pp. 2331–2334.

[12] M. Fujii, T. Suetsugu, K. Shinoda, and S. Mori, "Class E rectifier using thinned-out method," *IEEE Trans. Power Electron.*, vol. 12, no. 5, pp. 832–836, Sep. 1997.

[13] H. Koizumi, H. Sekiya, M. Matsuo, S. Mori, and I. Sasae, "Resonant dc/dc converter with class DE inverter and Class E rectifier using thinned-out method (deleting some of the pulses to the rectifier)," *IEEE Trans. Circuits Syst.*, vol. 48, no. 1, pp. 123–126, Jan. 2001.

[14] K. Sakuma and H. Koizumi, "Influence of junction capacitance of switching devices on class E rectifier," in *Proc. IEEE Int. Symp. Circuits Syst.*, May 2009, pp. 1965–1968.

[15] K. Fukui and H. Koizumi, "Class E rectifier using switch-controlled capacitor," in *Proc. IEEE Energy Convers. Congr. Expo.*, Sep. 2011, pp. 2332–2337.

[16] K. Fukui and H. Koizumi, "Class E rectifier with controlled shunt capacitor," *IEEE Trans. Power Electron.*, vol. 27, no. 8, pp. 3704–3713, Aug. 2012.

[17] Y. Kamito, K. Fukui, and H. Koizumi, "Class-E zero-voltage-switching rectifier using common-grounded multi-step controlled-shunt capacitor," in *Proc. IEEE Energy Convers. Congr. Expo.*, Sep. 2012, pp. 4203–4208.

[18] Y. Kamito, K. Fukui, and H. Koizumi, "An analysis of the class-E zero-voltage-switching rectifier using the common-grounded multistep-controlled shunt capacitor," *IEEE Trans. Power Electron.*, vol. 29, no. 9, pp. 4807–4819, Sep. 2014.

[19] M. K. Kazimierczuk and J. Jóźwik, "Class E zero-voltage-switching rectifier with a series capacitor," *IEEE Trans. Circuits Syst.*, vol. 36, no. 6, pp. 926–928, Jun. 1989.

[20] M. K. Kazimierczuk and K. Puczko, "Class E low dv/dt synchronous rectifier with controlled duty ratio and output voltage," *IEEE Trans. Circuits Syst.*, vol. 38, no. 10, pp. 1165–1172, Oct. 1991.

[21] M. K. Kazimierczuk and W. Szaraniec, "Analysis of class E rectifier with a series capacitor," *IEEE Trans. Circuits Syst.*, vol. 139, no. 3, pp. 269–276, Jun. 1992.

[22] A. Ivaşcu, M. K. Kazimierczuk, and Ş. Bîrcă-Gălăţeanu, "Class E resonant low dv/dt rectifier," *IEEE Trans. Circuits Syst.*, vol. 39, no. 8, pp. 604–613, Aug. 1992.

[23] M. K. Kazimierczuk, B. Tomescu, and A. Ivaşcu, "Class E resonant rectifier with a series capacitor," *IEEE Trans. Circuits Syst.*, vol. 41, no. 12, pp. 885–890, Dec. 1994.

[24] Ş. Bîrcă-Gălăţeanu and J.-L. Cocquerelle, "Class E half-wave low dv/dt rectifier operating in a range of frequencies around resonance," *IEEE Trans. Circuits Syst.*, vol. 42, no. 2, pp. 83–94, Feb. 1995.

[25] Ş. Bîrcă-Gălăţeanu, "Low peak current class E resonant full-wave low dv/dt rectifier driven by a voltage generator," in *Proc. Power Electron. Spec. Conf.*, Charleston, SC, USA, Jun. 1999, pp. 469–474.

[26] J. Jóźwik, and M. K. Kazimierczuk, "Class E zero-current-switching rectifier with a parallel inductor," in *Proc. IEEE Nat. Aerosp. Electron. Conf.*, May 1989, pp. 233–239.

[27] M. K. Kazimierczuk and J. Jóźwik, "Analysis and design of class E zero-current-switching rectifier," *IEEE Trans. Circuits Syst.*, vol. 37, no. 8, pp. 1000–1009, Aug. 1990.

[28] J. Jóźwik and M. Kazimierczuk, "Analysis and design of class-E^2 dc/dc converter," *IEEE Trans. Ind. Electron.*, vol. 37, no. 2, pp. 173–183, Apr. 1990.

[29] A. Reatti, "Analysis and design of a current-driven two-inductor ZCS low di_D/dt full-wave rectifier," *IEEE Trans. Circuits Syst.*, vol. 43, no. 9, pp. 745–759, Sep. 1996.

[30] M. K. Kazimierczuk and J. Jóźwik, "Class E zero-current-switching rectifier with a series inductor," in *Proc. 32nd Midwest Symp. Circuits Syst.*, Urbana, IL, USA, Aug. 1989, pp. 788–791.

[31] M. K. Kazimierczuk and W. Szaraniec, "Analysis of class E low di/dt rectifier with a series inductor," *IEEE Trans. Aerosp. Electron. Syst.*, vol. 29, no. 1, pp. 278–287, Jan. 1993.

[32] A. Ivaşcu, M. K. Kazimierczuk, and Ş. Bîrcă-Gălăţeanu, "Class E resonant low di/dt rectifier," in *Proc. Inst. Elect. Eng. G*, *Circuit Devices Syst.*, vol. 140, no. 6, pp. 417–423, Dec. 1993.
[33] A. Ivaşcu and Ş. Bîrcă-Gălăţeanu, "Class E half-wave low di/dt rectifier operating at frequencies around resonance," in *Proc. Power Electron. Spec. Conf.*, Jun. 1995, pp. 743–749.
[34] D. C. Hamill, "Half bridge class DE rectifier," *Electron. Lett.*, vol. 31, no. 22, pp. 1885–1886, Oct. 1995.
[35] D. C. Hamill, "Class DE inverters and rectifiers for dc-dc conversion," in *Proc. IEEE 27th Annu. Power Electron. Spec. Conf.*, Jun. 1996, pp. 854–860.
[36] K. N. Bateson, "Class DE dc-dc converters," in *Proc. 6th Workshop Comput. Power Electron.*, Jul. 1998, pp. 119–125.
[37] C. Ekkaravarodome, A. Nathakaranakule, and I. Boonyaroonate, "Single-stage fluorescent lamps electronic ballast using class-DE low dv/dt rectifier for power-factor correction," in *Proc. 7th Int. Conf. Power Electron. Drive Syst.*, Nov. 2007, pp. 1194–1198.
[38] C. Ekkaravarodome, A. Nathakaranakule, and I. Boonyaroonate, "Single-stage electronic ballast using class-DE low-dv/dt current-source-driven rectifier for power-factor correction," *IEEE Trans. Ind. Electron.*, vol. 57, no. 10, pp. 3405–3414, Oct. 2010.
[39] K. Fukui and H. Koizumi, "Half-wave class DE low dv/dt rectifier," in *Proc. IEEE Asia Pacific Conf. Circuits Syst.*, Dec. 2012, pp. 69–72.
[40] Y. Minami and H. Koizumi, "Class DE current driven low di/dt rectifier," in *Proc. IEEE Int. Symp. Circuits Syst.*, Jun. 2014, pp. 105–108.
[41] T. Misawa, K. Fukui, and H. Koizumi, "Zero current switching type class DE rectifier," in *Proc. IEEE 38th Annu. Conf. Ind. Electron.*, Oct. 2012, pp. 858–863.
[42] K. Jin, Z. Liu, X. Yu, and X. Ren, "A self-driven current-doubler-rectifier three-level converter with integrated magnetics," *IEEE Trans. Ind. Electron.*, vol. 29, no. 7, pp. 3604–3615, Jul. 2014.
[43] N. O. Sokal and A. D. Sokal, "Class E—A new class of high-efficiency tuned single-ended switching power amplifiers," *IEEE J. Solid-State Circuits*, vol. SC-10, no. 3, pp. 168–176, Jun. 1975.
[44] R. Redl, B. Molnár, and N. O. Sokal, "Class E resonant regulated dc/dc power converters: Analysis of operation and experimental results at 1.5 MHz," *IEEE Trans. Power Electron.*, vol. PE-1, no. 2, pp. 111–120, Apr. 1986.
[45] R. Redl, B. Molnár, and N. O. Sokal, "Small-signal dynamic analysis of regulated class E dc/dc converters," *IEEE Trans. Power Electron.*, vol. PE-1, no. 2, pp. 121–128, Apr. 1986.
[46] M. K. Kazimierczuk and X. T. Bui, "Class E dc/dc converters with an inductive impedance inverter," *IEEE Trans. Power Electron.*, vol. 4, no. 1, pp. 124–135, Jan. 1989.
[47] M. K. Kazimierczuk and X. T. Bui, "Class E dc/dc converters with a capacitive impedance inverter," *IEEE Trans. Ind. Electron.*, vol. 36, no. 3, pp. 425–433, Aug. 1989.
[48] ERA91-021 data-sheet. (2013). [Online]. Available: http://pdf1.alldatasheet.jp/datasheet-pdf/view/61214/FUJI/ERA91-02.html

Yutaro Minami (S'14) received the B.E. degree in electrical engineering from the Tokyo University of Science, Tokyo, Japan, in 2014, where he is currently working toward the M.E. degree.

His research interests include high-frequency rectifiers and resonant dc/dc power converters.

Hirotaka Koizumi (S'98–M'01) was born in Tokyo, Japan, in 1970. He received the B.E., M.E., and Ph.D. degrees in electrical engineering from Keio University, Yokohama, Japan, in 1993, 1995, and 2001, respectively.

From 1995 to 2001, he was an Electrical Engineer with Tokyo Electric Power Company Inc., Tokyo. From 1998 to 2001, he was with the Graduate School, Keio University, Tokyo. From 2001 to 2007, he was with Tokyo University of Agriculture and Technology, Tokyo, as a Research Associate. Since April 2007, he has been with Tokyo University of Science, Tokyo, where he is currently a Professor. His research interests include photovoltaic systems, high-frequency high-efficiency tuned power amplifiers, resonant dc/dc power converters, dc/ac inverters, and high-frequency rectifiers.

Dr. Koizumi is a Member of the Institute of Electrical Engineers of Japan and the Institute of Electronics, Information, and Communication Engineers of Japan. From May 2008 to May 2010, he was the Secretary of the IEEE Circuits and Systems Society Power Systems and Power Electronic Circuits Technical Committee. From May 2012 to May 2013 and from May 2013 to May 2014, he was the Chair and the Past Chair of the IEEE Circuits and Systems Society Power and Energy Circuits and Systems Technical Committee.